Inorg. Chem. **2007**, *46*, 11254–11265

Inorganic Chemistry
Article

Synthesis, Structure, and Magnetic Behavior of Bis(2-amino-5-fluoropyridinium) Tetrachlorocuprate(II)

Lixin Li and Mark M. Turnbull*

Carlson School of Chemistry and Biochemistry, Clark University, 950 Main Street,
Worcester, Massachusetts 01610

Christopher P. Landee

Department of Physics, Clark University, 950 Main Street, Worcester, Massachusetts 01610

Joaquim Jornet, Mercè Deumal, and Juan J. Novoa*

Department of Physical Chemistry, University of Barcelona, Martí i Franquès 1,
Barcelona, 08028, Spain

Jan L. Wikaira

Department of Chemistry, University of Canterbury, Private Bag 4800,
Christchurch, New Zealand

Received August 20, 2007

Reaction of $CuCl_2$ with 2-amino-5-fluoropyridine and HCl in aqueous solution yields bis(2-amino-5-fluoropyridinium) tetrachlorocuprate(II), $(5FAP)_2CuCl_4$, (**1**). The complex crystallizes in the monoclinic space group $P2_1/c$ with cell dimensions $a = 6.926(7)$ Å, $b = 21.73(2)$ Å, $c = 10.911(10)$ Å, $\beta = 100.19(2)°$, $V = 1616(3)$ Å^3, and $R_1 = 0.0424$ based on 2640 independent reflections. The crystal packing shows that each tetrachlorocuprate ion has four nearest-neighbor Cu(II) ions through three types of Cu–Cl···Cl–Cu potential magnetic interactions: one short Cl···Cl distance ($d_1 = 3.657$ Å) and two longer Cl···Cl distances ($d_2 = 4.073$ Å) that form a layered distorted honeycomb structure. The third nearest neighbor ($d_3 = 4.239$ Å) links these layers into a three-dimensional structure. Both powder and single-crystal magnetic susceptibility measurements on **1**, over the temperature range of 1.8–325 K, show significant antiferromagnetic interactions. Attempts to analyze the data using a variety of models showed a best fit to the strong-rung ladder model, with $2J_{rung} = -17.170(14)$ and $2J_{rail} = -5.94(5)$ K [–11.92(1) and –4.13(3) cm^{-1}, respectively] for the powder, although a comparable result is obtained using an alternate chain model. However, neither of these two models is compatible with a layered distorted honeycomb crystal packing structure. A first-principles bottom-up theoretical study using the 165 K crystallographic data reproduces the macroscopic properties and reveals that at low temperature the crystal has a 3D magnetic topology (all three magnetic pathways are significant) and a singlet ground state.

Introduction

Over the past several decades the study of magnetism on low-dimensional systems has been of major interest and played an important role in the understanding of phase transitions and critical phenomena.[1] This interest has increased continuously due to the discovery of high-temperature superconducting materials, where the superconductivity is thought to be propagated through low-dimensional antiferromagnetic networks.[2,3] The existence of strong antifer-

---

* To whom correspondence should be addressed. E-mail: mturnbull@clarku.edu.

(1) Pelissetto, A; Vicari, E. *Phys. Rep.* **2002**, *368*, 549–727.
(2) Dagotto, E.; Rice, T. M. *Science* **1996**, *271*, 618–623.
(3) Anderson, P. W.; Baskaran, G.; Zou, Z.; Hsu, T. *Phys. Rev. Lett.* **1987**, *58*, 2790–2793.

10.1021/ic701645y CCC: $37.00 © 2007 American Chemical Society
Published on Web 11/17/2007

romagnetic intraplanar interactions with very weak interaction in the third dimension has been demonstrated by experimental investigations of superconductors such as La_2CuO_4.[4] In general, an antiferromagnetic lattice can be described by the following Hamiltonian

$$\hat{H} = -2 \sum_{A,B} J_{AB} \hat{S}_A \cdot \hat{S}_B \tag{1}$$

where $\hat{S}_A$ and $\hat{S}_B$ are the spin operators acting on radicals A and B; A runs over all sites, and B runs over the Ath site's neighbors. In cases where the magnetic exchange is not isotropic, the Hamiltonian must be modified to take account of the different values of the exchange in different directions as determined by the crystal structure.

One class of antiferromagnets contains cooperative singlet ground states, separated from the lowest lying triplets by energy gaps Δ. The gaps can arise from single-ion anisotropy as in $NiCl_2-4SC(NH_2)_2$,[5] singlet−triplet splitting within antiferromagnetic copper dimers [such as $TlCuCl_3$[6] and Cs_2CuCl_4],[7] spin ladders [$(C_5H_{12}N_2)_2Cu_2Cl_4$],[8] or the Haldane gap found in antiferromagnetic $S = 1$ Heisenberg chains.[9] The existence of the energy gap prevents these magnets from spontaneously ordering. However, application of an external field will close the gap at a critical field $H_{C1} = \Delta/g\mu_B$ and ultimately drive the system to saturation at the upper critical field H_{C2}. For $H > H_{C1}$, the presence of 3D interactions will lead to an ordered state at sufficiently low temperature. The phase diagrams of these systems are generic, independent of the origin of the gap.[10]

At $T = 0$ and in a field equal to H_{C1}, $S = 1$ magnons can be created at low energy cost and will produce a net magnetization. This process can be described[11,12] as the Bose−Einstein condensation (BEC) of the triplet magnets, implying that the details of the BEC process can be explored in systems other than ultracold gases. Due to the 3D antiferromagnetic interactions, a Néel order perpendicular to the applied field is induced. Increasing the field beyond H_{C1} increases the transverse moment and enhances the Néel temperature according to the power law $H_C(T) = H_{C1} + T^{\alpha}$ with α being a universal exponent. However, experimental studies[13,14] have found different exponents. The differences may be due to the presence of competing interactions in the system or the existence of a first-order transition at H_{C1}. There is a clear need for additional spin-singlet ground-state magnets which have been well characterized for further study of field-induced ordering.

Copper(II) coordination compounds are an especially attractive source of model systems in the study of low-dimensional systems since a large body of theoretical work exists,[15−17] and analysis of data for complicated structures may be readily obtained for use in magneto-structural correlations. The d^9 configuration of the Cu(II) ion has one unpaired electron ($S = 1/2$), and the nearly quenched orbital angular momentum of the Cu(II) ion provides a g factor close to 2, suggesting the absence of any large internal magnetic fields.

We have been interested in the design and preparation of low-dimensional magnetic lattices with antiferromagnetic properties for some time. One route for generating such lattices is via crystal packing of transition-metal-ion complexes. Following this method we have been preparing and studying a series of compounds with the formula $A_2[MX_4]$, where A is an organic cation, usually a protonated base, M is a transition-metal ion (usually Cu^{2+}), and X is a halide (Cl, Br).[18,19] Complexes of tetrahalocuprates with different organic cations provide a wealth of structural types as the packing of the CuX_4^{2-} ions is highly dependent upon the size and shape of the organic cations. A number of these compounds have also been prepared using the same synthetic method where the cation is a protonated N-heterocycle such as pyridine,[20] morpholine,[21] or pyrimidine.[22] The magnetic exchange in these compounds is essentially mediated by the direct overlap between the orbitals of the halide ions of the MX_4^{2-} pseudo-tetrahedra, and these overlaps are determined by the crystal packing. We have been studying the use of 5-substituted-2-aminopyridines (5-SAP) as potential bases for this purpose. We are interested especially in how the size and shape of the 5-substituent of the 2-aminopyridine affects the symmetry of the crystal lattice and separation between the MX_4^{2-} ions. Over the past decade we have reported our

---

(4) Birgeneau, R. J. *Am. J. Phys.* **1990**, *58*, 28−40.

(5) Zvyagin, S. A.; Wosnitza, J.; Batista, C. D.; Tsukamoto, M.; Kawashima, N.; Krzystek, J.; Zapf, V.S.; Jaime, M.; Oliveira, N. F., Jr.; Paduan-Filho, A. *Phys. Rev. Lett.* **2007**, *98*, 047205/1−4.

(6) Oosawa, A.; Ishii, M.; Tanaka, H. *J. Phys. Condens. Matter* **11**, 265−71 (1999).

(7) Coldea, R.; Tennant, D. A.; Habicht, K.; Smeibidl, P.; Wolters, C.; Tylczynski, A. *Phys. Rev. Lett.* **2002**, *88*, 137203/1−4.

(8) Chaboussant, G.; Fagot-Revurat, Y.; Julien, H.-H.; Hanson, M. E.; Berthier, C.; Horvatic, M.; Lévy, L. P.; Piovesana, O. *Phys. Rev. Lett.* **1998**, *80*, 2713−16.

(9) Renard, J. P.; Verdaguer, M.; Regnault, L. P.; Erkelens, W. A. C.; Rossat-Mignod, J.; Stirling, W. G. *Europhys. Lett.* **1987**, *3*, 945−52.

(10) Carlin, R. L. *Magnetochemistry*; Springer-Verlag: New York, 1986; pp 7−8, 136.

(11) Giamarchi, T.; Tsvelik, A. M. *Phys. Rev. B* **1999**, *59*, 11398−11407.

(12) Nikuni, T.; Oshikawa, M.; Oosawa, A.; Tanaka, H. *Phys. Rev. Lett.* **2000**, *84*, 5868−71.

(13) Oosawa, A.; Aruga Katori, H.; Tanaka, H. *Phys. Rev. B* **2001**, *63*, 134416/1−4.

(14) Radu, T.; Wilhelm, H.; Yushankhai, V.; Kovrizhin, D.; Coldea, R.; Tylczynski, Z.; Lühmann, T.; Steglich, F. *Phys. Rev. Lett.* **2005**, *95*, 127202/1−4.

(15) Hatfield, W. E.; Helms, J. H. *Mater. Sci.* **1992**, *17*, 21−31.

(16) Ueda, K.; Takamizawa, S.; Mori, W.; Kubo, S.; Yamaguchi, K. *Mol. Cryst. Liq. Cryst. Sci. Technol., Sect. A: Mol. Crys. Liq. Cryst.* **1997**, *306*, 33−40.

(17) *Quantum Magnetism*; Schollwöck, U., Richter, J., Farnell, D. J. J., Bishop, R. F., Eds.; Springer-Verlag: New York, 2004.

(18) Matsumoto, T.; Miyazaki, Y.; Albrecht, A. S.; Landee, C. P.; Turnbull, M. M.; Sorai, M. *J. Phys. Chem. B* **2000**, *104*, 9993−10000.

(19) Turnbull, M. M.; Galeriu, C.; Giantsidis, J.; Landee, C. P. *Mol. Cryst. Liq. Cryst. Sci. Technol., Sect. A: Mol. Crys. Liq. Cryst.* **2002**, *376*, 469−476.

(20) Willett, R. D.; Awwadi, F.; Butcher, R.; Huddad, S.; Twamley, B. *Cryst. Growth Des.* **2003**, *3*, 301−311.

(21) Zhou, P.; Drumheller, J. E.; Rubenacker, G. V.; Halvorson, K.; Willett, R. D. *J. Appl. Phys.* **1991**, *69*, 5804−5806.

(22) (a) Manfredini, T.; Pellacani, G. C.; Bonamartini-Corradi, A.; Battaglia, L. P.; Gaurini, G. G. T.; Guisti, J. G.; Willett, R. D.; West, D. X. *Inorg. Chem.* **1990**, *29*, 2221−2228. (b) Zanchini C.; Willett, R. D. *Inorg. Chem.* **1990**, *29*, 3027−3030. (c) Pon, G.; Willet, R. D.; Prince, B. A.; Robinson, W. T.; Turnbull, M. M. *Inorg. Chim. Acta* **1997**, *255*, 325−334.

work with 2-amino-5-iodopyridinium (5-IAP),[23] 2-amino-5-bromopyridinium (5-BAP),[24] 2-amino-5-chloropyridinium (5-CAP),[25] and 2-amino-5-methylpyridinium (5-MAP).[25] To extend the family of 5-SAP compounds, we report the synthesis, crystal structure, and magnetic characterization of the fluoro-substituted complex (5-FAP)$_2$CuCl$_4$ [5-FAP = 2-amino-5-fluoropyridinium].

Experimental Section

2-Amino-5-fluoropyridine was purchased from Aldrich and used as received. Copper(II) chloride (anhydrous) was purchased from Aesar and used as received. IR spectra were recorded as KBr pellets on a Perkin-Elmer Paragon 500 spectrophotometer (4000−550 cm^{-1}) and referenced to polystyrene.

Synthesis of (5-FAP)$_2$CuCl$_4$. 2-Amino-5-fluoropyridine (0.336 g, 3mmol) was slurried in 15.0 mL of water. Concentrated hydrochloride acid (0.939 g) was added dropwise to the mixture with stirring and a light yellow solution resulted. A solution of CuCl$_2$ (0.200 g, 1.5mmol) in 18.0 mL of water was added to the above solution. After stirring for 0.5 h, the resulting dark brown solution was transferred to a small vial and allowed to evaporate slowly at room temperature. After nearly 1 month, long, green, rod-shaped crystals suitable for X-ray analysis were isolated by vacuum filtration, washed quickly with cold ethanol, and dried under vacuum overnight to give 0.319 g (49%). No attempt was made to maximize the yield. IR (KBr): 3391 (m), 3306 (m), 3186 (m), 3050 (m), 1676 (m), 1630 (vs), 1552(s), 1467 (m), 1353 (m), 1260 (m), 1136 (w), 777 (s), 688 (w), 511 (w) cm^{-1}.

X-ray Crystallography. Crystals of compound **1** were removed from the container; a suitable size (0.31 × 0.40 × 0.58 mm) crystal was selected, attached to a glass fiber, and mounted on a Bruker/Siemens SMART system (Mo Kα radiation, $\lambda = 0.71073$ Å) using φ and ω scans for data collection at 165 K. Cell parameters were determined using SMART[26] software and refined using SAINTPlus.[27] Data reduction and corrections were performed using SAINTPlus.[27] Absorption corrections were made via SADABS.[28] The structure was solved via direct methods using SHELXS97[29] and refined via least squares using SHELXL97.[29] Hydrogen atoms bonded to carbon atoms were placed in calculated positions and refined as a riding model with fixed isotropic values. The positions of H atoms bonded to nitrogen atoms were refined with anisotropic thermal parameters. Details of the data collection parameters and crystallographic information for complex **1** are provided in Table 1. The structure has been deposited with the CCDC (CCD #619501). A Bruker D8 powder X-ray diffractometer was used to verify that powder samples used for magnetic measurements were the same phase as the single crystal.

Table 1. Crystal Data and Structure Refinement for **1**

empirical formula	C$_{10}$H$_{12}$N$_4$F$_2$Cl$_4$Cu
fw	431.58
T (K)	165(2)
wavelength (Å)	0.71073
cryst syst	monoclinic
space group	$P2_1/c$
a (Å)	6.926(7)
b (Å)	21.73(2)
c (Å)	10.911(10)
β (deg)	100.19(2)
V (Å^3)	1616(3)
Z	4
density (calcd) (mg/mm^3)	1.773
abs coeff (mm^{-1})	2.208
final R^a indices [$I > 2\sigma(I)$]	R$_1$ = 0.0424, wR$_2$ = 0.1108
R indices (all data)	R$_1$ = 0.0521, wR$_2$ = 0.1335
largest diff. peak and hole (e Å^{-3})	0.72 and −0.80

[a] $R_1 = \sum||F_o| - |F_c||/\sum|F_o|$; $wR_2 = \{\sum[w(F_o^2 - F_c^2)^2]/\sum[w(F_o^2)^2]\}^{1/2}$.

Magnetic Data Collection. Magnetic susceptibility data for complex **1** were measured on a Quantum Design MPMS-XL SQUID magnetometer. Crystals of **1** were powdered and packed into a #3 gelatin capsule. There was no hysteresis observed in the magnetization of the sample as a function of applied field from 0 to 50 kOe at 1.8 K. The moment is linear with the applied field up to at least 10 000 Oe. Susceptibility data of the same powdered sample and a carefully selected single crystal [2 × 2 × 1.5 mm, 15.6 mg] were taken over the temperature range from 1.8 to 325 K in an applied field of 1000 Oe.

The data were corrected for temperature-independent paramagnetism of the Cu(II) ion ($\chi = 60 \times 10^{-6}$ emu·mol^{-1}) and for the diamagnetism of the constituent atoms using Pascal's constants (-219.5×10^{-6} emu·mol^{-1}). The high-field magnetization data were collected using a vibrating sample magnetometer (Lake Shore model 7600 VSM), a helium cryostat, and the 325 kOe Bitter magnet at the National High Magnetic Field Laboratory in Tallahassee, FL. Temperatures were determined by calibrated Cernox resistors and the vapor pressure of the helium bath.

Theoretical Methods. We performed a first-principles bottom-up theoretical study[30] of the magnetic interactions of the (5-FAP)$_2$CuCl$_4$ crystal. This procedure computes the macroscopic magnetic properties using the crystal structure as the only input, that is, without making any starting assumptions about the nature or strength of the magnetic interactions established between the radicals of the crystal. This first-principles bottom-up approach is an improvement in comparison to the usual first-principles studies on radical−radical magnetic interactions, where only the first two steps of the first-principles bottom-up procedure are performed, without connecting the data obtained with the macroscopic properties. The approach can be described as the successive realization of the following four steps.

Step 1: Analysis of the crystal structure to find all unique radical−radical pairs present in the crystal. The only spin carrying units in the (5-FAP)$_2$CuCl$_4$ crystal are the CuCl$_4^{2-}$ anions. Each CuCl$_4^{2-}$ unit is a doublet radical by means of the unpaired electron of Cu(II), which does not belong entirely to the Cu(II) atom since it is also shared over the Cl atoms due to spin polarization. The magnetic interactions between CuCl$_4^{2-}$ units are through space (also called direct magnetic interactions). Previous studies involving Cu(II) radicals have shown that radical−radical magnetic interactions become negligible with Cu···Cu distances above 8.5 Å.[31a,b] Thus,

---

(23) (a) Giantsidis, J.; Galeriu, C.; Landee, C. P.; Turnbull, M. M. *J. Coord. Chem.* **2002**, *55*, 795−803. (b) Landee, C. P.; Turnbull, M. M.; Galeriu, C.; Giantsidis, J.; Woodward, F. M. *Phys. Rev. B*: *Condens. Matter* **2001**, *63*, 100402/1−4.

(24) (a) Giantsidis, J. B. A. Thesis, Clark University, Worcester, MA, May 2002. (b) Woodward, F. M.; Landee, C. P.; Giantsidis, J.; Turnbull, M. M.; Richardson, C. *Inorg. Chim. Acta* **2001**, *324*, 324−330.

(25) (a) Hammer, P. R.; Dender, D. C.; Reich, D. H.; Albrecht, A. S.; Landee, C. P. *J. Appl. Phys.* **1997**, *81*, 4615−4617. (b) Woodward, F. M.; Albrecht, A. S.; Wynn, C. M.; Landee, C. P.; Turnbull, M. M. *Phys. Rev. B: Condens. Matter* **2002**, *65*, 144412/1−13.

(26) *SMART, Bruker Molecular Analysis Research Tool*; Bruker AXS: Madison, WI, 1997−1998.

(27) *SAINTPlus, Data Reduction and Correction Program*; Bruker AXS: Madison, WI, 1999.

(28) Sheldrick, G. M. *SADABS v.2.01: an empirical absorption correction program*; Bruker AXS Inc.: Madison, WI, 1999.

(29) Sheldrick, G. M. *SHELXS97; Program for the Solution of Crystal Structures*; University of Gottingen: Gottingen, Germany, 1997.

(30) Deumal, M.; Bearpark, M. J.; Novoa, J. J.; Robb, M. A. *J. Phys. Chem. A* **2002**, *106*, 1299−1315.

Scheme 1

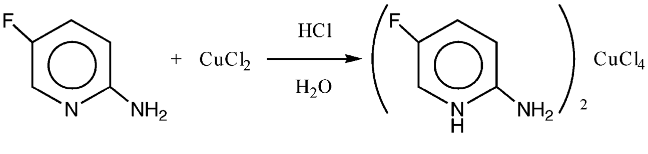

1

when looking for all unique radical pairs, only those radical pairs showing a Cu···Cu distance smaller than 10 Å were taken into account (this cutoff includes all first nearest neighbors and the closest second nearest neighbors).

Step 2: Computation of the radical−radical magnetic interactions (J_{AB}) for each unique radical−radical pair found in the crystal. There are only two possible states for the radical−radical pairs selected in step 1: a singlet and a triplet state. Therefore, the value of J_{AB} for each pair is obtained from the energy difference between the open-shell singlet and triplet states of the selected anion−radical pairs (at their 165 K crystal geometry). The computations were done using the embedded cluster approximation,[31] i.e., surrounding each anion−radical pair by their four nearest counterions (previous calculations indicate that this allows simulation of the main effects induced by the Madelung field in the singlet and triplet states). We compute the singlet and triplet energies using the B3LYP functional,[32] an Ahlrich-pVDZ[33] basis set for Cu, and a 6-31+G(d)[34] basis set for the remaining atoms as implemented in Gaussian03.[35] The broken symmetry approach[36] was used to compute the open-shell singlet for a proper description of this state. Within this approximation the value of J_{AB} for the Heisenberg Hamiltonian (1) is obtained as $2J_{AB} = 2(E_{BS}^{S} - E^{T})$, where E^{T} is the energy of the triplet state and E_{BS}^{S} is the energy of the singlet state computed using the broken symmetry approach (the expression for J_{AB} derives from the original broken-symmetry equations when the SOMO orbitals of the two radicals do not overlap, which is the usual situation in through-space magnetic interactions). Our experience indicates that this expression gives results closer to the experimental values than alternative ones where projection is used. It is worth pointing out here that there has been some controversy about the use of projection when computing the values of the J_{AB} parameters using the broken-symmetry approach within the DFT context (for detailed discussions, see refs 37).

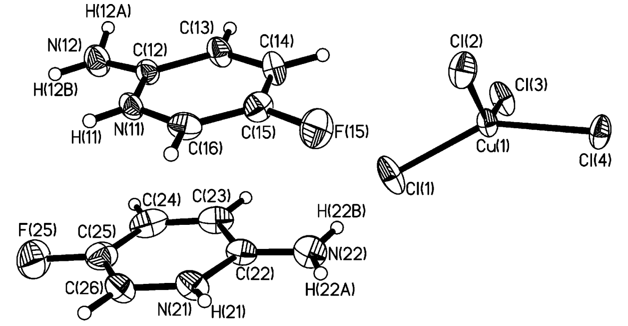

Figure 1. Asymmetric unit for $(FAP)_2CuCl_4$ (**1**) showing 50% probability thermal ellipsoids.

Table 2. Selected Bond Lengths (Å) and Bond Angles (deg) for $(5\text{-}FAP)_2CuCl_4$[a]

Cu(1)−Cl(1)	2.225(2)	Cu(1)−Cl(2)	2.250(2)
Cu(1)−Cl(3)	2.2681(18)	Cu(1)−Cl(4)	2.2371(17)
C(15)−F(15)	1.344(4)	C(25)−F(25)	1.349(5)
Cl(4)···Cl(4A)	3.657(3)	Cl(1)···Cl(3B)	4.073(3)
Cl(2)···Cl(4D)	4.239(3)[b]		
Cl(1)−Cu(1)−Cl(2)	98.01(6)	Cl(1)−Cu(1)−Cl(3)	96.06(7)
Cl(1)−Cu(1)−Cl(4)	146.90(5)	Cl(2)−Cu(1)−Cl(3)	140.92(5)
Cl(4)−Cu(1)−Cl(2)	93.80(6)	Cl(4)−Cu(1)−Cl(3)	93.92(8)
Cu(1)−Cl(4)···Cl(4A)#1	137.54(6)	Cu(1)−Cl(1)···Cl(3B)	149.81(4)
Cu(1)−Cl(3)···Cl(1C)#2	149.55(6)	Cu(1)−Cl(4)···Cl(4A)−Cu(1A)	180.0
Cu(1)−Cl(1)···Cl(3B)−Cu(1B)#3	96.0		

[a] See Figure 3a for $CuCl_4^{2-}$ atom numbering. #1: 1 − *x*, 1 − *y*, 1 − *z*. #2: *x*, 3/2 − *y*, 1/2 + *z*. #3: *x*, 3/2 − *y*, *z* − 1/2. [b] Not shown in Figure 3a. Cl(4D) lies in an adjacent plane.

Step 3: Determination of the magnetic topology of the crystal and its minimal magnetic model space. The magnetic topology is defined as the network of connections that the non-negligible J_{AB} magnetic interactions (i.e., $J_{AB} > |0.05|\ cm^{-1}$) establish among the radicals. The minimal model space is the smallest subset of radicals that includes all non-negligible J_{AB} magnetic interactions in a ratio similar to that found in the infinite crystal. Its extension along the three crystallographic axes must obviously reproduce the magnetic topology of the infinite crystal. Consequently, when a proper minimal magnetic model space is selected, the computed macroscopic properties must converge toward the experimental result.

Step 4: Calculation of the macroscopic magnetic properties of the crystal using adequate statistical mechanics expressions. Once the J_{AB} values are computed in step 2, we can diagonalize the matrix representation of the appropriate Heisenberg Hamiltonian. This

---

(31) The original reference on embedded cluster models is given in Ellis, D. E.; Benesh, G. A.; Byrom, E. *Phys. Rev. B* **1977**, *16*, 3308−3313. For a recent application, see: (a) Shapiro, A.; Landee, C. P.; Turnbull, M. M.; Jornet, J.; Deumal, M.; Novoa, J. J.; Robb, M. A. *J. Am. Chem. Soc.* **2007**, *129*, 952−959. (b) Deumal, M.; Giorgi, G.; Robb, M. A.; Turnbull, M. M.; Landee, C. P.; Novoa, J. J. *Eur. J. Inorg. Chem.* **2005**, 4697−4706.

(32) (a) Becke, A. D. *Phys. Rev. A: At. Mol. Opt. Phys.* **1988**, *38*, 3098−3100. (b) Lee, C.; Yang, W.; Parr, R. G. *Phys. Rev. B: Condens. Matter* **1988**, *37*, 785−789. (c) Becke, A. D. *J. Chem. Phys.* **1993**, *98*, 5648−5652.

(33) Ahlrichs' pVDZ basis set: Schafer, A.; Horn, H.; Ahlrichs, R. *J. Chem. Phys.* **1992**, *97*, 2571−2577.

(34) 6−31+G(d) split-valence basis set: (a) Hariharan, P. C.; Pople, J. A. *Theor. Chim. Acta* **1973**, *28*, 213−222. (b) Francl, M. M.; Petro, W. J.; Hehre, W. J.; Binkley, J. S.; Gordon, M. S.; DeFrees, D. J.; Pople, J. A. *J. Chem. Phys.* **1982**, *77*, 3654−3665.

(35) Frisch, M. J.; Trucks, G. W.; Schlegel, H. B.; Scuseria, G. E.; Robb, M. A.; Cheeseman, J. R.; Montgomery, J. A., Jr.; Vreven, T.; Kudin, K. N.; Burant, J. C.; Millam, J. M.; Iyengar, S. S.; Tomasi, J.; Barone, V.; Mennucci, B.; Cossi, M.; Scalmani, G.; Rega, N.; Petersson, G. A.; Nakatsuji, H.; Hada, M.; Ehara, M.; Toyota, K.; Fukuda, R.; Hasegawa, J.; Ishida, M.; Nakajima, T.; Honda, Y.; Kitao, O.; Nakai, H.; Klene, M.; Li, X.; Knox, J. E.; Hratchian, H. P.; Cross, J. B.; Bakken, V.; Adamo, C.; Jaramillo, J.; Gomperts, R.; Stratmann, R. E.; Yazyev, O.; Austin, A. J.; Cammi, R.; Pomelli, C.; Ochterski, J. W.; Ayala, P. Y.; Morokuma, K.; Voth, G. A.; Salvador, P.; Dannenberg, J. J.; Zakrzewski, V. G.; Dapprich, S.; Daniels, A. D.; Strain, M. C.; Farkas, O.; Malick, D. K.; Rabuck, A. D.; Raghavachari, K.; Foresman, J. B.; Ortiz, J. V.; Cui, Q.; Baboul, A. G.; Clifford, S.; Cioslowski, J.; Stefanov, B. B.; Liu, G.; Liashenko, A.; Piskorz, P.; Komaromi, I.; Martin, R. L.; Fox, D. J.; Keith, T.; Al-Laham, M. A.; Peng, C. Y.; Nanayakkara, A.; Challacombe, M.; Gill, P. M. W.; Johnson, B.; Chen, W.; Wong, M. W.; Gonzalez, C.; Pople, J. A. *Gaussian 03*, Revision C.02; Gaussian, Inc.: Wallingford, CT, 2004.

(36) (a) Noodleman, L. *J. Chem. Phys.* **1981**, *74*, 5737−5746. (b) Noodleman, L.; Davidson, E. R. *Chem. Phys.* **1986**, *109*, 131−143.

(37) (a) Ruiz, E.; Alvarez, S.; Cano, J.; Polo, V. *J. Chem. Phys.* **2005**, *123*, 164110/1−7. (b) Adamo, C.; Barone, V.; Bencini, A.; Broer, R.; Filatov, M.; Harrison, N. M.; Illas, F.; Malrieu, J. P.; Moreira, I. P. R. *J. Chem. Phys.* **2006**, *124*, 107101/1−3.

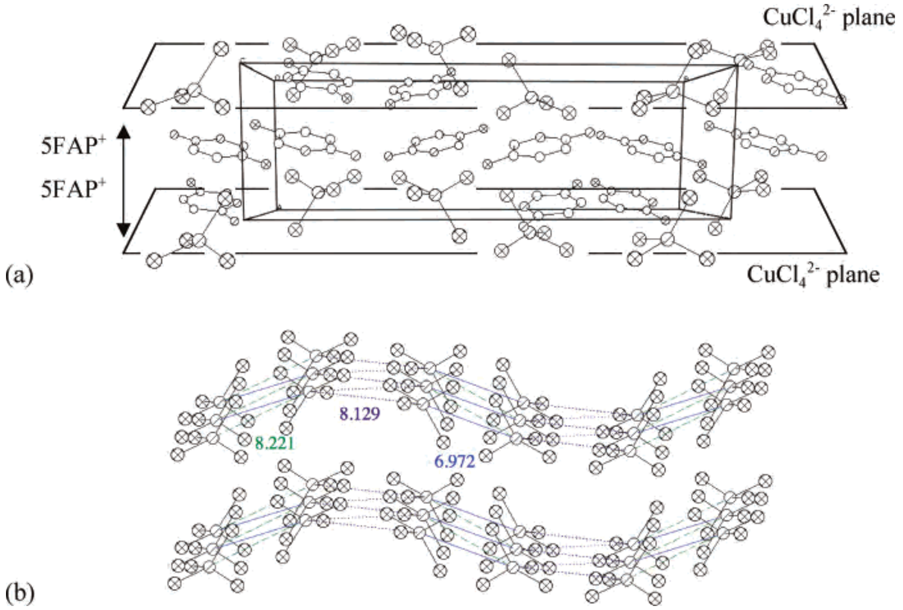

Figure 2. (a) View of the packing pattern in which the organic cations $5FAP^+$ separate the $CuCl_4^{2-}$ ions into layers (viewed parallel to the *c* axis; the *b* axis is horizontal; H atoms are omitted for clarity). (b) $CuCl_4^{2-}$ packing, indicating the shortest three contact distances between Cu atoms within the *bc* plane (organic cations are omitted).

Table 3. Hydrogen Bonds for **1** [Å and deg][a]

D−H···A	*d*(D−H)	*d*(H···A)	*d*(D···A)	∠(DHA)
N12−H12B···Cl3#1	0.85(5)	2.40(5)	3.227(5)	164(5)
N12−H12A···Cl3#2	0.86(5)	2.42(6)	3.272(4)	169(4)
N22−H22B···Cl1	0.87(6)	2.37(6)	3.232(5)	169(5)
N22−H22A···Cl2#3	0.79(5)	2.48(6)	3.247(5)	162(5)

[a] Symmetry transformations used to generate equivalent atoms: (#1) $x - 1, -y, z - 1$; (#2) $x - 1, -y + 3/2, z - 1/2$; (#3) $-x, -y + 1, -z$.

representation is computed on the basis of spin eigenfunctions of the minimal magnetic model space. We used the following form of the Heisenberg Hamiltonian

$$\hat{H} = -2\sum_{\mathrm{A,B}} J_{\mathrm{AB}}\left(\hat{S}_{\mathrm{A}}\cdot\hat{S}_{\mathrm{B}} + \frac{1}{4}\hat{I}_{\mathrm{AB}}\right) \tag{2}$$

where $\hat{I}_{\mathrm{AB}}$ is the identity operator while $\hat{S}_{\mathrm{A}}$ and $\hat{S}_{\mathrm{B}}$ are the spin operators acting on radicals A and B. Notice that the energy spectrum computed using either Hamiltonian 1 or 2 results in the same energy differences between different eigenvalues. Using these eigenvalues, the macroscopic magnetic properties are computed using the proper statistical mechanics expressions. Notice that the size of the matrix representation of the Heisenberg Hamiltonian increases with the number of doublet radical N centers as $N!/[(N/2)!(N/2)!]$. Currently, we can reach up to 16 different doublet centers.

This approach is an objective four-step procedure for connecting the microscopic to the macroscopic magnetic information, step 3 being the key step for this micro to macro connection. We must stress the fact that this first-principles bottom-up procedure benefits from well-known theoretical methods from chemistry (step 2) and physics (step 4) as part of a global strategy to study molecular magnetism. It is *bottom-up* because the macroscopic magnetic properties are obtained from the microscopic radical−radical magnetic interactions, i.e., it connects the macroscopic magnetic properties with their microscopic origin (the J_{AB} values) in a numerically accurate and unbiased form. It is also *first-principles* because the J_{AB} values are computed by first-principles calculations. Its only input is the crystal geometry, and no assumptions are made about the nature of the radical−radical interactions found in the crystal. This first-principles bottom-up strategy has been successfully applied to a series of crystals representative of a variety of macroscopic behaviors.[38]

Results and Analysis

Crystal Structure. Reaction of copper(II) chloride with 2 equivalents of 2-amino-5-fluoropyridine in aqueous HCl solution gave $(5\text{-FAP})_2CuCl_4$ (**1**) as shown in Scheme 1.

Single crystals suitable for X-ray diffraction were harvested by slow evaporation of the solution over a period of 5 weeks. Crystals of **1** are monoclinic in the space group $P2_1/c$. The asymmetric molecule unit is shown in Figure 1. Relevant bond lengths and angles are given in Table 2.

The corresponding bond lengths and angles of the two rings are slightly different with bond lengths varying from 1.299 (N21−C22) to 1.419 Å (C12−C13) and bond angles from 114° (N21−C22−C23) to 132° (C22−N21−C26). The C−F bonds are 1.344(4) and 1.349(5) Å, as expected for an aromatic C−F bond.[39,40] The organic cations are nearly planar with a small mean deviation from the planes of 0.0439 and 0.0159 Å for the N(11) and N(21) rings, respectively. The two rings are also nearly coplanar with an angle of 4.3° between their mean planes.

The bond lengths of $CuCl_4^{2-}$ anions are unremarkable and comparable with similar compounds,[23a,24a,25a] varying from 2.225 to 2.268 Å. The bond angles show significant distortion

---

(38) (a) Deumal, M.; Bearpark, M. J.; Robb, M. A.; Pontillon, Y.; Novoa, J. J. *Chem. Eur. J.* **2004**, *10*, 6422−6432. (b) Deumal, M.; Mota, F.; Bearpark, M. J.; Robb, M. A.; Novoa, J. J. *Mol. Phys.* **2006**, *104*, 857−873. (c) Jornet, J.; Deumal, M.; Ribas-Ariño, J.; Bearpark, M. J.; Robb, M. A.; Hicks, R. G.; Novoa, J. J. *Chem. Eur. J.* **2006**, *12*, 3995−4005.

(39) Shishkov, I. F.; Khristenko, L. V.; Samdal, S.; Gundersen, S.; Volden, H. V.; Vilkov, L. L. *J. Mol. Struct.* **2004**, *693*, 133−140.

(40) Chou, Y.; Huang, S.; Koner, T.; Lee, G.; Huang, Y.; Mohanta, S.; Wei, H. *Inorg. Chem.* **2004**, *43*, 2759−2761.

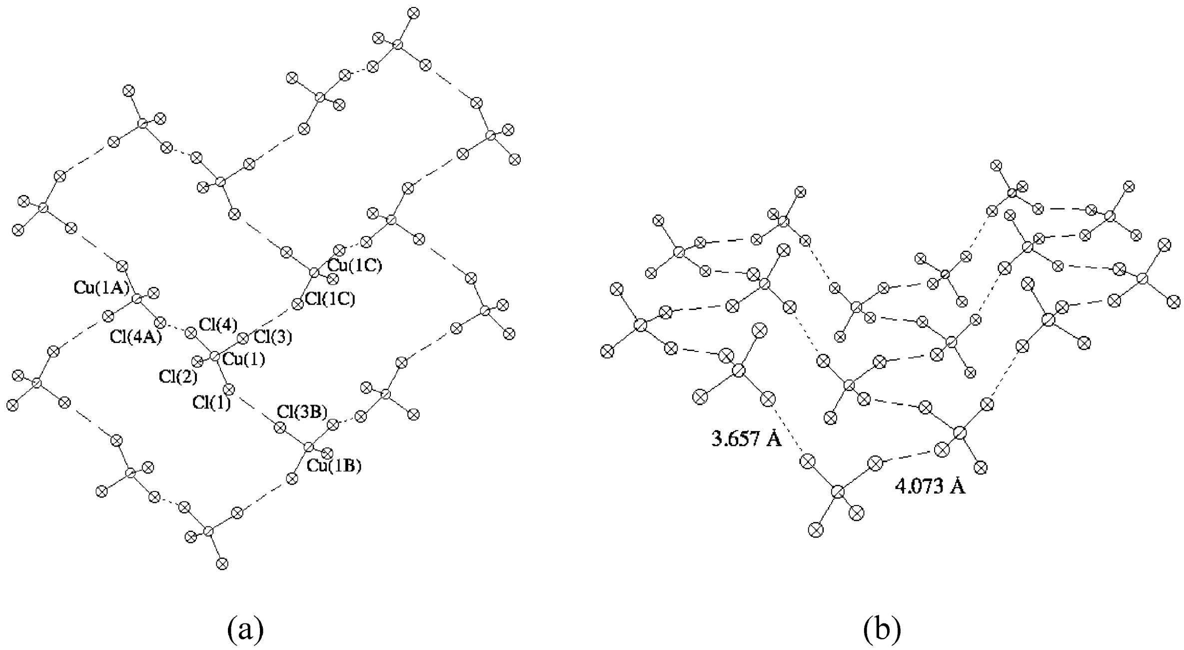

(a) (b)

Figure 3. $CuCl_4^{2-}$ contacts through Cl···Cl, forming a distorted honeycomb structure by one nearest (Cl(4)···Cl(4A) at 3.657 Å (dotted line)) and two next nearest (Cl(1)···Cl(3) at 4.073 Å (dashed line)) neighbors in the layer. Top (a) and lateral (b) views of a given *bc* plane.

Table 4. Results Using Different Models for the Powder Data[a]

models	dimer	unif. chain	square layer	strong-rail ladder	alt. chain	strong-rung ladder
C (emu·K/mol)	0.391(3)	0.300(15)	0.496(7)	0.46(23)	0.412(4)	0.4168(5)
2*J* (K)	−17.5(1)	−20.4(5)	−10.63(10)	−14.8(3)	−18.149(5)	−17.170(14)
2*J*′ (K)				2.8(2.5)	−7.717(4)	−5.94(5)
P (%)	5.31(8)	665(55)	−0.48(14)	−0.034(21.9)	1.90(1)	0.0192(1)
R^2	1.49E-7	1.39E-6	4.70E-7	7.62E-7	1.72E-9	1.46E-9

[a] *P* = % paramagnetic impurity; R^2 = goodness of fit.

Table 5. Results of the Best Fit with Antiferromagnetic Strong-Rung Ladder Model for All the Magnetic Data[a]

sample	*x* axis	*y* axis	*z* axis	powder
C (emu·K/mol)	0.4144(4)	0.4218(8)	0.4128(5)	0.4168(5)
2*J* (rung) (K)	−17.57(1)	−17.68(2)	−17.62(1)	−17.170(14)
2*J* (rail) (K)	−5.05(4)	−4.92(7)	−4.97(5)	−5.94(5)
P (%)	0.405(7)	0.0018(1)	0.397(7)	0.0192(1)
R^2	1.14E-9	3.19E-9	2.17E-9	1.46E-9

[a] *P* = % paramagnetic impurity; R^2 = goodness of fit, *x*, *y*, *z* are the three orthogonal directions based on the shape of the single crystal.

from an ideal tetrahedron as expected for CuX_4^{2-} ions, with a mean trans angle[41] of 143.9(1)°.

The packing structure of **1** can be described as composed of $CuCl_4^{2-}$ anion layers separated by the organic cations, as shown in Figure 2a. Viewed parallel to the *c* axis, $CuCl_4^{2-}$ anion layers are isolated by two organic cation layers. The $CuCl_4^{2-}$ anions in the layers are not strictly on flat sheets but rather form zigzag layers as shown in Figure 2b. The structure is stabilized by hydrogen bonding between the amino groups and chloride ions as shown in Table 3 (not shown in Figure 2). Although there are possible hydrogen bonds via the pyridinium hydrogen atoms, they are at larger distances (≥3.2 Å) and thus may be significantly weaker.

Analysis of the chloride···chloride contacts in the structure reveals three potential magnetic pathways (Figure 3a). The shortest contacts occur via inversion-related chloride ions with a separation of 3.657 Å (Cl(4)···Cl(4A)), significantly shorter than seen in similar compounds.[23−25] The Cu(1)−Cl(4)···Cl(4A) and Cl(4)···Cl(4A)−Cu(1A) angles are both 137.5°, and the dihedral angle Cu(1)−Cl(4)···Cl(4A)−Cu(1A) is 180° as required by symmetry. The next nearest neighbor Cl···Cl contacts occur between Cl(1) and Cl(3) [4.073 Å, with a Cu(1)−Cl(1)···Cl(3B) angle of 149.81(4)° and Cl(1)···Cl(3B)−Cu(1B) of 149.55(6)°]. The dihedral angles of these connections are 96°, which is not an effective angle for magnetic superexchange according to magnetostructural correlations.[41] Thus, within the layer, each $CuCl_4^{2-}$ anion has one short nearest neighbor contact and two next nearest neighbor contacts, forming a distorted honeycomb structure as shown in Figure 3.

However, unlike some of the other 5-SAP compounds,[23−25] the $CuCl_4^{2-}$ layers are not well isolated by the organic cations. The shortest Cl···Cl contacts between layers (Cl(4D)···Cl(2)) are 4.239 Å, only slightly longer than the next nearest neighbor contacts within the layers. All other intermolecular Cl···Cl distances are longer than 5 Å. The overall packing of the $CuCl_4^{2-}$ anions can be described as linked, distorted honeycomb layers.

Magnetic Data. Magnetization data as a function of field were collected for a powder of complex **1** at 1.8 K from 0 to 50 kOe. A smooth curve was obtained, and the moment varied linearly with the applied field up to 10 kOe.

---

(41) Turnbull, M. M.; Landee, C. P.; Wells, B. M. *Coord. Chem. Rev.* **2005**, *249*, 2567−2576.

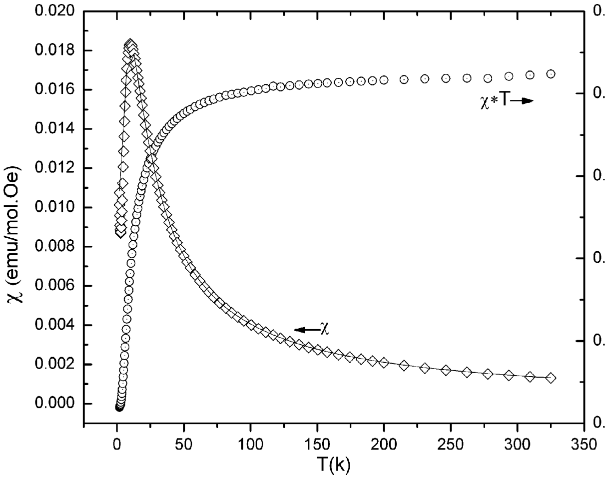

Figure 4. Plot of χ_{mol} vs T (◇) and χT vs T (○) for **1**. The solid line is the fit to the strong-rung ladder model with parameters $2J_{\mathrm{rung}} = -17.170(14)$ K and $2J_{\mathrm{rail}} = -5.94(5)$ K [$-11.92(1)$ and $-4.13(3)$ cm^{-1}, respectively].

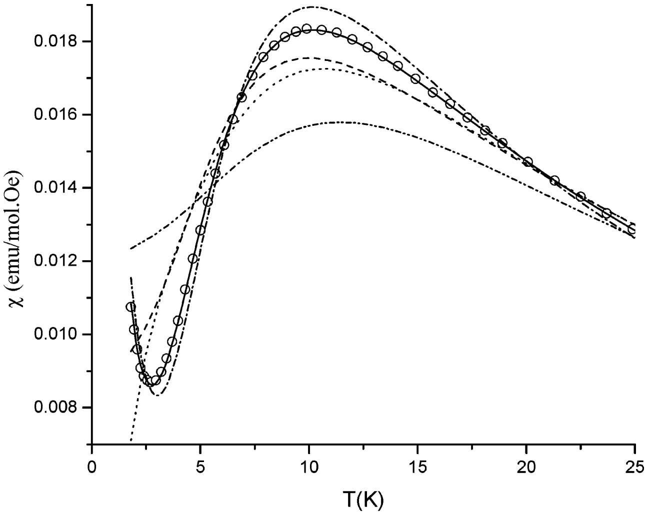

Figure 5. Fits to the magnetic susceptibility data using different models. Dash-dot, dimer; solid, strong-rung; dash, square layer; dot, strong-rail; dash-dot-dot, uniform chain. The alternating-chain model is virtually superimposable on the strong-rung model and not shown for clarity. The percent paramagnetic impurity was fixed to zero when a negative value was obtained in the fit.

Magnetization data as a function of temperature were collected at 1000 Oe from 1.8 to 325 K. Figure 4 shows the results plotted as χ vs T and χT vs T. A maximum of $\chi_{\mathrm{mol}} = 1.83 \times 10^{-3}$ emu/(mol·Oe) near 11 K is observed in the curve of χ vs T and clearly indicates the presence of antiferromagnetic interactions. A fit to $1/\chi_{\mathrm{mol}}$ from 1.8 to 325 K yields a Curie−Weiss $\theta = -10.5$ K. The antiferromagnetic properties are also reflected in the χT vs T plot, which shows downward curvature at low temperature.

Due to the lack of models for either a honeycomb structure or a 3D system with different exchange constants, a variety of known models were used to attempt to fit the magnetic data. The best fit for the powder magnetic data was obtained when using a strong-rung ladder model, which is shown by the solid line in Figure 4, giving $2J_{\mathrm{rung}} = -17.170(14)$ K [$-11.92(1)$ cm^{-1}], $2J_{\mathrm{rail}} = -5.94(5)$ K [$-4.13(3)$ cm^{-1}], and Curie constant of 0.4168(5) with a very small paramagnetic impurity ($P = 0.0192\%$). However, a comparably good fitting of the powder magnetic data was obtained when using an alternating chain model, giving $2J_{\mathrm{d}} = -18.149(5)$ K

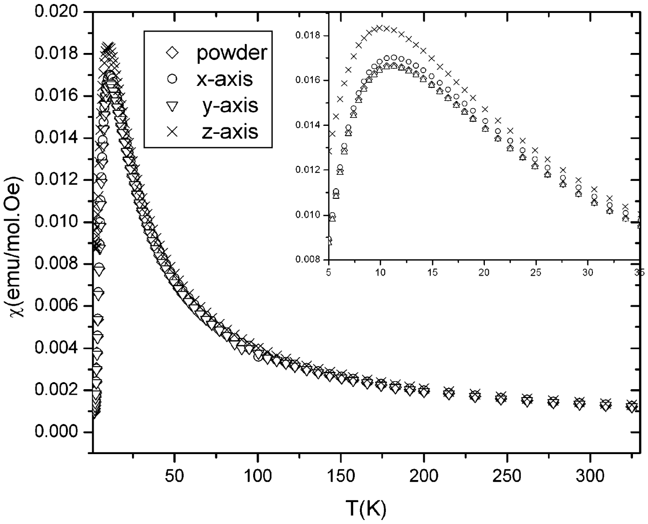

Figure 6. χ vs T for three different directions of a 15.7 mg single crystal and the powder sample. The insert is an expansion of the region from 5 to 35 K.

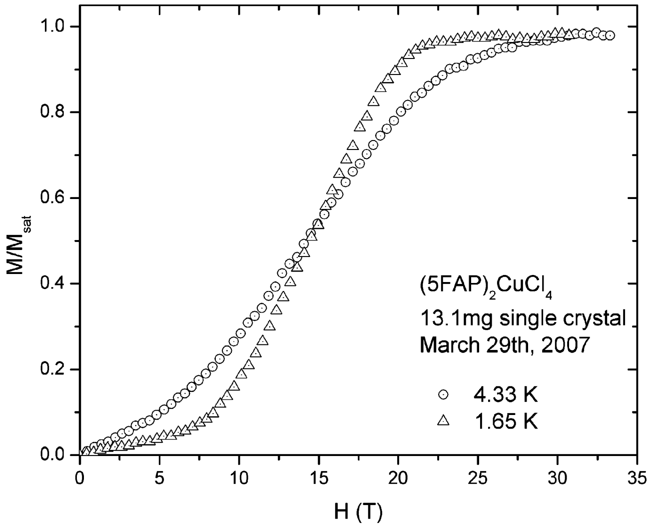

Figure 7. Magnetic moment as a function of applied field of complex **1** at 4.33 and 1.65 K (4 T/min scan rate).

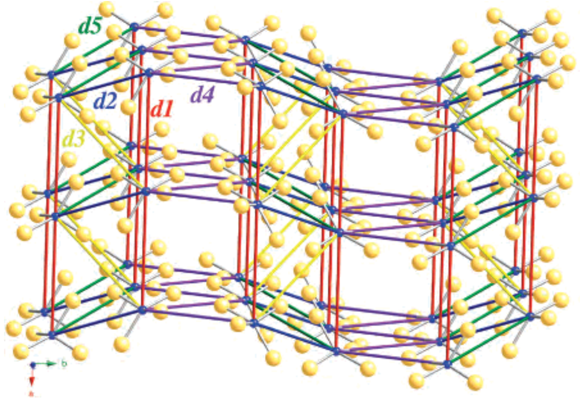

Figure 8. Selected $Cl_4Cu\cdots CuCl_4$ pairs with Cu···Cu distance shorter than 10.0 Å, whose magnetic strength should be evaluated. Lines in different colors represent all five possible *di*, $i = 1-5$, magnetic interactions.

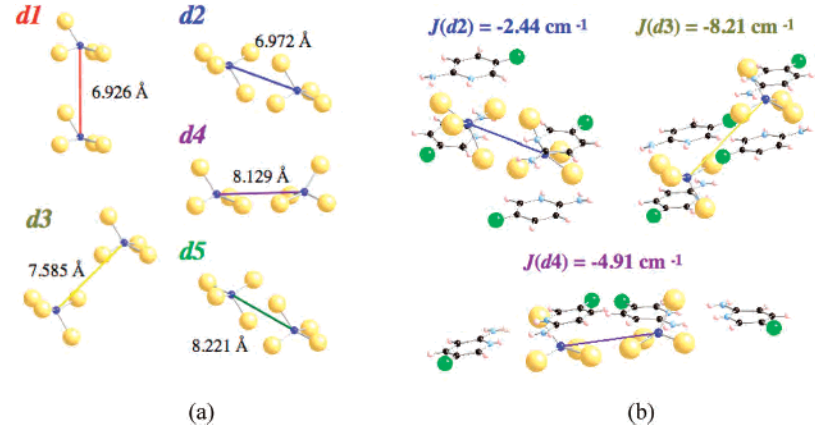

Figure 9. (a) Different *di* anion$_2$ radical pair models whose $Cl_4Cu\cdots CuCl_4$ distance is given inset. (b) *di* anion$_2$−cation$_4$ cluster models with non-negligible magnetic interactions. Notice antiferromagnetic $J(di)$ numerical values are given in cm^{-1}. The values in thermal units are −3.5, −11.8, and −7.1 K, respectively.

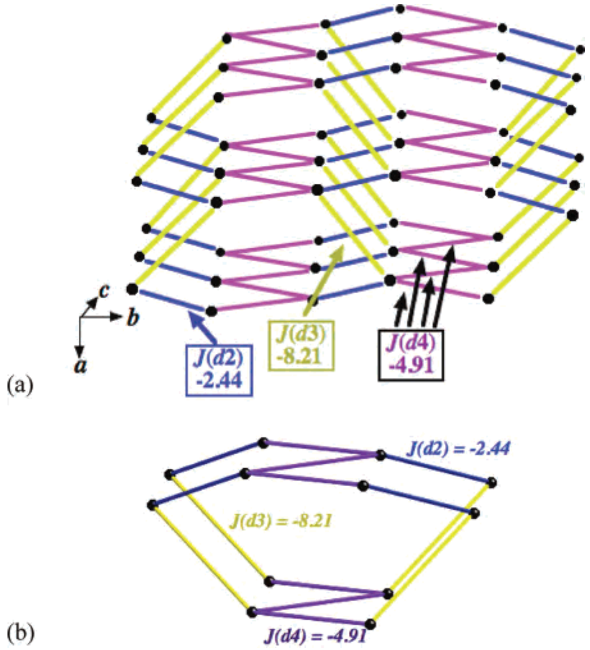

Figure 10. (a) Three-dimensional magnetic topology (consisting of interacting two-dimensional hexagonal-shaped layers along the *c* axis; each 2D unit consists of two $J(d2)$, two $J(d3)$, and two $J(d4)$ magnetic contacts, which then interacts with adjacent layers through $J(d4)$ interactions). (b) 3d12s minimal magnetic model consisting of a 12 radical site three-dimensional model. Calculated exchange values are −2.44 (−3.5 K), −8.21 (−11.8 K), and −4.91 cm^{-1} (−7.1 K).

[−12.60(3) cm^{-1}] and $2J = -7.717(4)$ K [−5.36(3) cm^{-1}] with a small paramagnetic impurity ($P = 1.90\%$). Poorer fits or unphysical values were obtained using other models. The results are listed in Table 4 and also shown in Figure 5.

Single-crystal magnetic data support the powder measurements. A crystal of 15.7 mg (2 × 2 × 1.5 mm) was chosen for the experiment. The measurements were made using three arbitrary orthogonal directions called *x*, *y*, *z* axes separately (the *x*, *y*, and *z* axes may or may not be the same as the *a*, *b*, and *c* axes of the X-ray structure). All three directions show maxima near 11 K in the plots of χ_{mol} vs T, as seen in the powder sample of **1**. Figure 6 shows χ as a function of temperature for the three different directions of the single crystal and also for the powder sample. All data sets compare well, and only small differences are seen between the *z* direction and any other direction or powder as shown in the insert to Figure 6.

Analysis of the single-crystal data using a variety of known models also showed a best fit to the strong-rung ladder model, although that model has no physical meaning when compared to the packing structure and gave similar results to the powder sample as shown in Table 5.

From Table 5, we notice that the agreement for the rung exchange is much better than that in the rail direction. The goodness of fit is virtually the same for changes of several percent in the weaker interaction, while a comparable change in the strong interaction makes a major difference. In fact, the insensitivity of the goodness of fit to the weaker magnetic interaction is confirmed by theoretical calculations.[42]

At this point it was clear that the two best-fitting models obtained using the powder and single-crystal data (strong-rung ladder and alternating chain model) were not consistent with the known crystal structure for **1**. Thus, the J_{AB} values obtained from these fits should not be directly associated with real radical−radical magnetic interactions. Given this fact we decided to employ a first-principles bottom-up study to analyze the main issues related with the magnetic properties of **1**.

High-Field Magnetization Data. The molar magnetization as a function of applied field for a single crystal of $(5FAP)_2CuCl_4$ is shown in Figure 7 at 4.33 and 1.65 K. The data exhibit upward curvature, indicative of the low-dimensional nature of the sample, and saturate at approximately 20 T (200 kOe). In the low-temperature data set (1.65 K) a critical field at approximately 8 T (80 kOe) is also observed, which indicates that a gap exists between the singlet ground state and first excited triplet state. The singlet−triplet gap was determined to be approximately 11.3(5) K experimentally based on the equation[10] $\Delta = E_1 - E_0 = g\mu_B m_S H_{C1}$, where g is the gyromagnetic factor ($g =$

---

[42] Johnston, D. C.; Troyer, M.; Miyahara, S.; Lidsky, D.; Ueda, K.; Azuma, M.; Hiroi, Z.; Takano, M.; Isobe, M.; Ueda, Y.; Korotin, M. A.; Anisimov, V. I.; Mahajan, A. V.; Miller, L. L. Los Alamos National Laboratory, Preprint Archive, Condensed Matter (2000), 1−63, arXiv: cond-mat/0001147.

Table 6. Computed J_{AB} Values for Each Selected $Cl_4Cu\cdots CuCl_4$ Pair Shown in Figure 8 Using Both an $Anion_2$ Model and $Anion_2-Cation_4$ Model; the Most Significant Intermolecular Distances Are Also Given

dimer *di*	dCu⋯Cu/Å	d_{min}Cl⋯Cl/Å	J_{AB} (*di*) K (cm^{-1}) anion$_2$ model	J_{AB} (*di*) K (cm^{-1}) anion$_2$−cation$_4$ model
d1	6.926	5.087	−0.12 (−0.08)	
d2	6.972	4.239	−5.96 (−4.14)	−3.5 (−2.44)
d3	7.585	3.657	−37.15 (−25.80)	−11.8 (−8.21)
d4	8.129	4.073	−10.08 (−7.00)	−7.1 (−4.91)
d5	8.221	6.135	−0.04 (−0.03)	

2.11, calculated from the powder magnetic data), μ_B is the Bohr magneton, $m_s = -1$ for the lowest sublevel for the triplet excited state, and H_{c1} is the critical field.

Theoretical Calculations. We applied a first-principles bottom-up four-step strategy to study the magnetism of the $(5FAP)_2CuCl_4$ antiferromagnet using a crystal structure determined by X-ray at 165 K.

In Step 1, after analysis of the crystal packing in terms of Cu⋯Cu distances shorter than 10 Å, we found five pairs *d1−d5* whose magnetic strength should be evaluated: the relevant Cu⋯Cu distances ranging from 6.926 to 8.221 Å (see Figures 8 and 9a and Table 6). If all five pairs were non-negligible, the three-dimensional (3D) magnetic topology shown in Figure 8 would be obtained.

The J_{AB} values for each of the five radical pairs selected in Step 1 were then evaluated (Step 2) using neutral anion$_2$-cation$_4$ clusters rather than anion$_2$ clusters, as the former better reproduces the environment of the anions within the crystal.[21] The four $5FAP^+$ counterions selected were those presenting the shortest distances with the $CuCl_4^{2-}$ anions of the pair. The computed J_{AB} interactions are collected in Table 6. The values computed using the anion$_2$ clusters (Figure 9a) are always larger than those obtained with the anion$_2$-cation$_4$ clusters (Figure 9b), a fact that is mostly due to the compression effect induced by the cations in the shape of the orbitals of the anions. Notice that the anion$_2$cation$_4$ cluster model supports the argument on the magnetic exchange occurring via the nonbonding halide⋯halide contacts rather than any direct interactions between the metal ions. The strength of the exchange correlates well with the Cl⋯Cl distances but does not correlate at all with the Cu⋯Cu distances.

J(*d2*), *J*(*d3*), and *J*(*d4*) are the only non-negligible antiferromagnetic interactions with values of −3.5 (−2.44 cm^{-1}), −11.8 (−8.21 cm^{-1}), and −7.1 K (−4.91 cm^{-1}), respectively. They define a 3D magnetic topology (Step 3) of interacting 2D hexagonal-shaped layers (see Figure 10a). Each unit of the hexagonal-shaped layer consists of two *J*(*d2*), two *J*(*d3*), and two *J*(*d4*) magnetic contacts, which then interacts with the adjacent layers through *J*(*d4*) interactions. The most adequate minimal magnetic model for such 3D magnetic topology appears to be a three-dimensional 12 radical sites model (namely, 3d12s) formed by two interacting hexagonal-shaped units (see Figure 10b).

Using the three-dimensional 3d12s minimal magnetic model space we computed the variation of the magnetic susceptibility as a function of temperature (Step 4). As shown in Figure 11, there is a good qualitative and quantitative agreement between computed and experimental $\chi(T)$ and $\chi T(T)$ curves, except for the region of the maximum. Although this difference can be due to various factors, detailed studies in other crystals suggest that it is mostly due to the use of a 165 K crystal structure rather than a structure determined at a temperature closer to the region of magnetic interest. The singlet−triplet spin gap has been computed to be 6.03 cm^{-1} (8.68 K), in good accordance with the experimental value of 11.3 K. Therefore, we can conclude that the 3d12s minimal magnetic model space, which represents the 3D magnetic topology of Figure 10a, reproduces well the experimental macroscopic magnetic data for this crystal.

As mentioned before, the experimental magnetic susceptibility curve is best fit by low-dimensionality empirical models: the strong-rung ladder model (a predominantly 1D model) or the alternating chain model (a 1D model). Therefore, as a final test in our theoretical study of the magnetic properties of **1** we evaluated whether the experimental magnetic susceptibility curve could also be reproduced by 2D or 1D minimal magnetic model besides the 3d12s model. The first model tested was a 2D model obtained by turning off *J*(*d2*), the smallest J_{AB} in the Heisenberg Hamiltonian. This produced a set of isolated honeycomb layers (see Figures S2 and 12a). The second model tested was a 1D model obtained by turning off *J*(*d4*). This produced an isolated chain topology (see Figures S1 and 12a). The minimal magnetic models that best represent the 2D and 1D magnetic topologies of Figure 12a are named as 2d16s and 1d8s in Figure 12b (see Figure S1−S2). According to Figure 12c, none of them appropriately reproduces the shape of the experimental $\chi(T)$ curve: the 2d16s model does not go to zero when T goes to zero, while the 1d8s model goes to zero at $T > 0$ but fails to reproduce the position of the maximum.

Discussion

Halide−halide nonbonding contacts between CuX_4^{2-} ions have been known to propagate magnetic exchange for many years.[43] A number of parameters appear to affect the strength of the exchange, including the X⋯X distance, Cu−X⋯X angles, and Cu−X⋯X−Cu torsion angle.[41] Shorter X⋯X distances, larger Cu−X⋯X angles, and torsion angles near 0° and 180° correlate with larger antiferromagnetic exchange constants. The magnetic exchange interaction decreases

---

(43) (a) Block, R.; Jansen, L. *Phys. Rev. B: Condens. Matter* **1982**, *26*, 148−153. (b) Snively, L. O.; Haines, D. N.; Emerson, K.; Drumheller, J. E. *Phys. Rev. B: Condens. Matter* **1982**, *26*, 5245−5247. (c) Straatman, P.; Block, R.; Jansen, L. *Phys. Rev. B: Condens. Matter* **1984**, *29*, 1415−1418. (d) Marsh, W. E.; Hatfield, W. E.; Hodgson, D. J. *Inorg. Chem.* **1988**, *27*, 1819−1821.

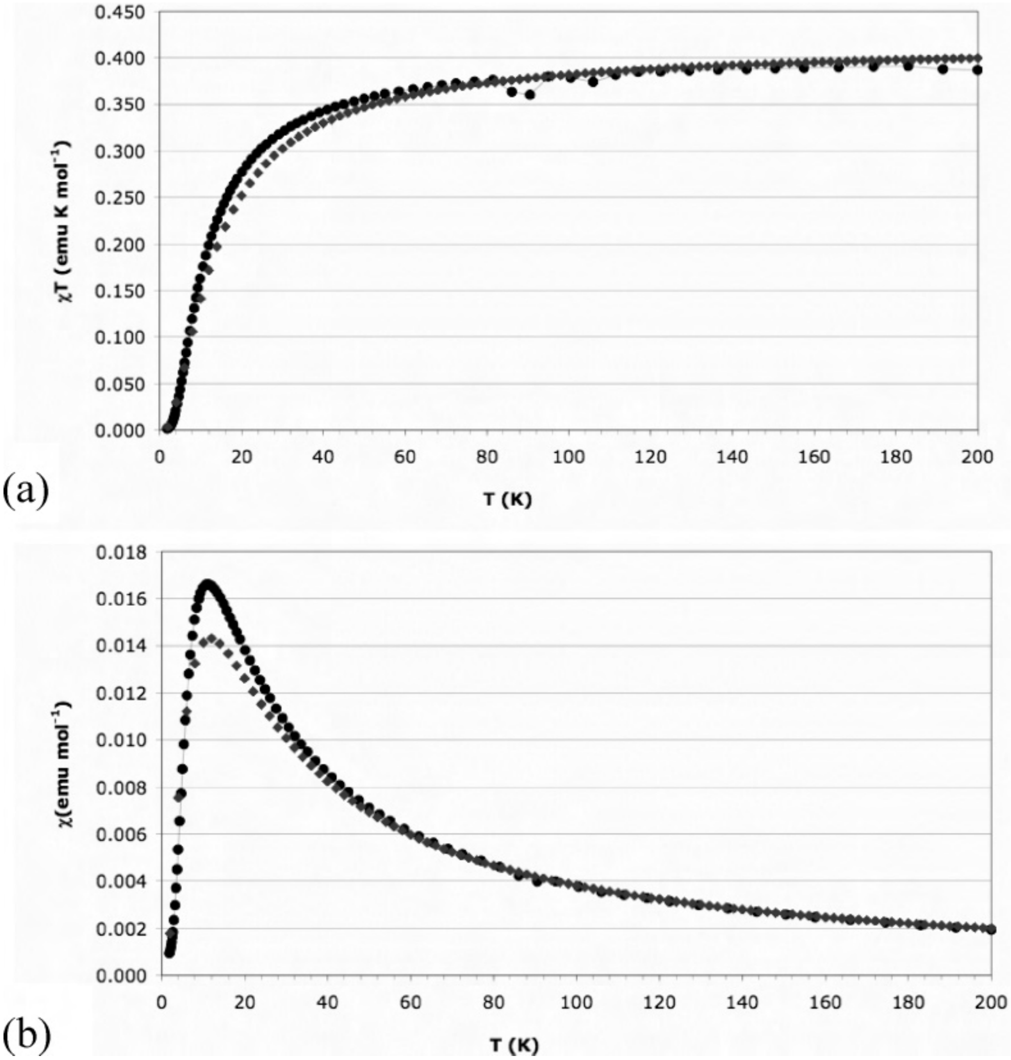

Figure 11. Computed (a) $\chi(T)$ (emu/mol-Oe) and (b) $\chi T(T)$ (emu-K/mol-Oe) curve for $(5FAP)_2CuCl_4$ crystal using a 3d12s minimal magnetic model (blue diamonds). The experimental curve (●) is also shown.

rapidly with the increase of the X···X distance, with $J \propto r^{-n}$, where the parameter n has been variously estimated to be between 10 and 12.[44]

The substituent in the 5-position on the 2-aminopyridine ring protrudes into the copper tetrahedra layer (see Figure 2a). The larger substituent forces the tetrahedra farther apart, increasing the X···X distance between adjacent tetrahedra and causing a decrease in the magnitude of the intralayer exchange interaction.[23−25] Therefore, a large exchange interaction is expected when using the small F atom as a substituent instead of Cl, Br, or I in the 5-position of the ring, if the packing motif is retained in the new structure. On the other hand, the copper anion layers are also separated by the organic cations. Therefore, if a small substituent is placed in the 5-position of the ring, the CuX_4^{2-} layers might be less separated and, thus, a larger interlayer exchange interaction should also be expected. Furthermore, a small change in the organic cation may also affect the packing structure of the crystal and hence the space group.

The magnetic susceptibility data show a best fit to a strong-rung ladder model, although that does not agree with the X-ray structure. By comparing the strong-rung ladder with the distorted honeycomb structure, we can find some topological similarities as shown in Figure 13. They both have three connections with their neighbors: two neighbors of one type and one neighbor of a second type. Although the fit is good, the question is still open: should we build a new superexchange magnetic simulation model for the honeycomb structure or more accurately a 3D model if we continue to consider the next shortest Cl···Cl distance, reflecting its own geometry instead of borrowing from other models. Complex **1** is an excellent example for such a study.

A first-principles bottom-up analysis of the $(5\text{-FAP})_2CuCl_4$ crystal discards the variety of known models that were used to fit the magnetic susceptibility data (see Table 4). The results from the present study corroborate the fact that although the best fit to the data is a strong-rung ladder

---

(44) (a) Snively, L. O.; Tuthill, G. F.; Drumheller, J. E. *Phys. Rev. B: Condens. Matter* **1981**, *24*, 5349−5355. (b) Bloch, D. *Phys. Chem. Solids* **1966**, *27*, 881−885.

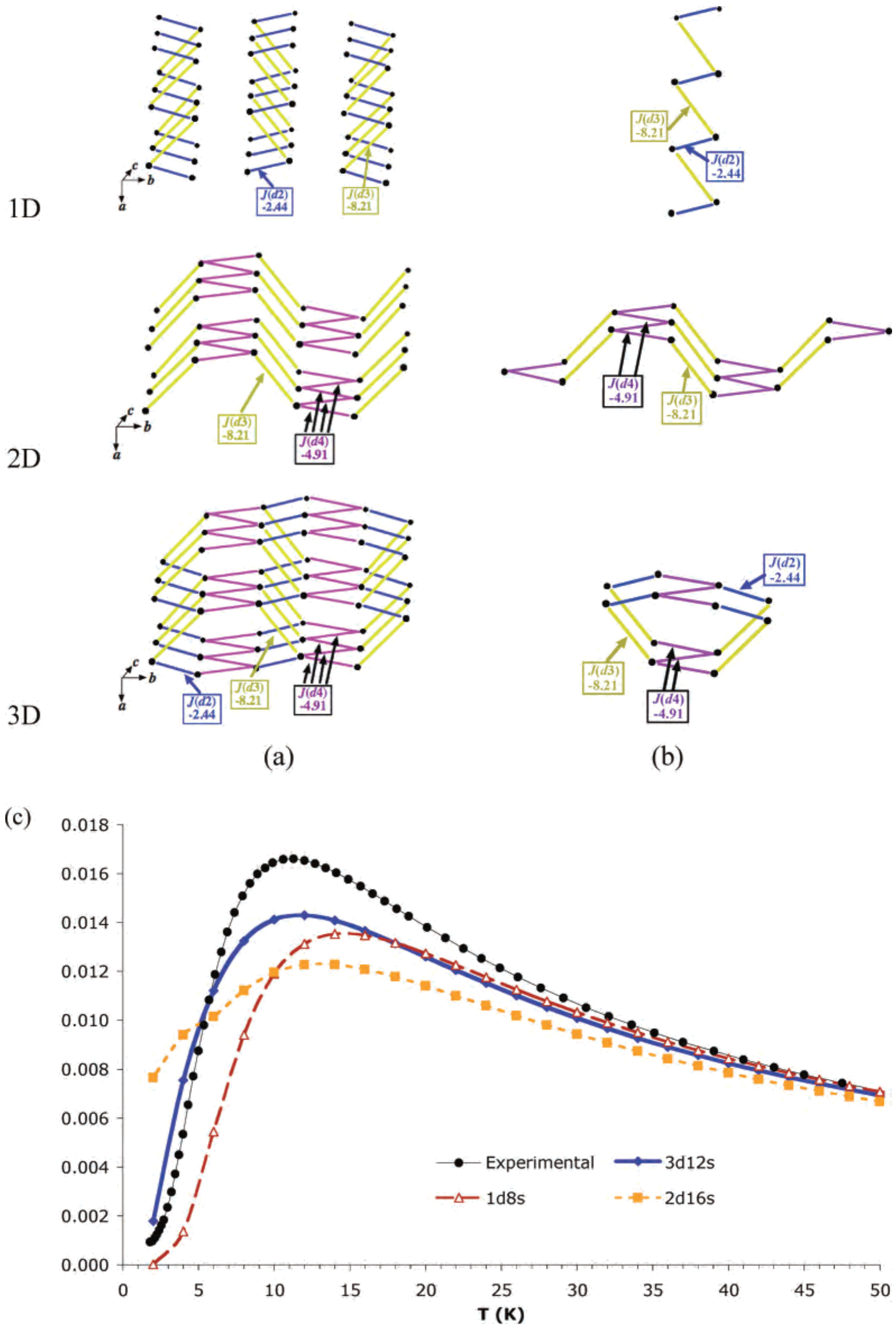

Figure 12. (a) 1D isolated chain magnetic topology resulting from turning off *J*(*d4*); 2D magnetic topology resulting from turning off *J*(*d2*) yields a set of isolated honeycomb layers; 3D magnetic topology resulting from applying a first-principles bottom-up analysis to $(5FAP)_2CuCl_4$ crystal. (b) Minimal magnetic models required for 1D−2D−3D magnetic topologies. (c) Simulated magnetic susceptibility $\chi(T)$ data using all three magnetic models. Comparison to experimental data is also shown. Calculated exchange values are −2.44 (−3.5 K), −8.21 (−11.8 K), and −4.91 cm^{-1} (−7.1 K).

model, it does not agree with the connectivity suggested by the X-ray structure. However, the analysis also precludes the linked distorted honeycomb layer motif pointed out from the crystal packing structure. According to Cl···Cl distances (see Figure 3 and Table 6), each honeycomb layer would result from the shortest Cl···Cl contacts at 3.66 and 4.07 Å, which can be identified with *d3* and *d4*, respectively. Any two such layers could then be connected through the next shortest Cl···Cl contact at 4.24 Å, which corresponds to *d2*. According to Table 6, although *d3* and *d4* have J_{AB} values of −8.21 and −4.91 cm^{-1} (−11.8 and −7.1 K), any *d2* contact has a −2.44 cm^{-1} (−3.5 K)

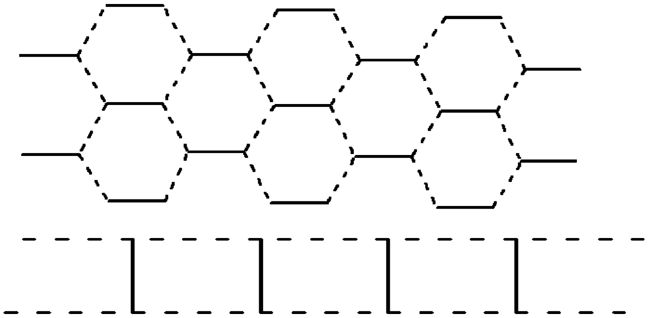

Figure 13. Topological similarity between honeycomb and ladder models. Both show two neighbors of one type (dashed line) and one neighbor of a second type (solid line).

non-negligible J_{AB} value. It follows that the resulting 3D magnetic topology is a consequence of the interplay of these three antiferromagnetic J_{AB} exchange interactions and, thus, cannot be inferred only from direct analysis of the crystal packing.

A series of simulations using alternative magnetic topologies (assuming one of the three J_{AB} values to be zero in each case) demonstrates the true three-dimensional nature of the material. Thus, our first-principles bottom-up procedure has proven its utility once more in understanding the mechanism of the magnetic interactions within a molecule-based material.

Conclusion

A new complex, $(5FAP)_2CuCl_4$ (**1**), has been synthesized and characterized by X-ray diffraction and magnetic susceptibility measurements. Along with other members of the $(5SAP)_2CuX_4$ family, it shows significant magnetic interactions through the nonbonding halide···halide exchange pathway. X-ray data analysis shows the copper tetrahedra anions packing as a distorted honeycomb layer by two types of short Cl···Cl connections. These layers are linked into a 3D structure via the next shortest Cl···Cl distance. Ab initio calculations clearly show that the most relevant parameter in determining the magnitude of such exchange is the distance between the halide ions rather than the copper(II) centers. Both single-crystal and powder magnetic susceptibility data show the antiferromagnetic nature of the complex. Attempts to analyze the data using a variety of known models showed a best fit to the strong-rung ladder model with $2J_{\mathrm{rung}} = -17.170(14)$ K [$-11.92(1)$ cm^{-1}] and $2J_{\mathrm{rail}} = -5.94(5)$ K [$-4.12(3)$ cm^{-1}], although that model does not agree with the crystal packing structure. In addition, it is clear that it is not only the geometrical arrangement of Cl···Cl contacts that decides the magnitude of the magnetic interaction. The 5-FAP$^+$ counterions play a role in such magnetic interaction via 5-FAP$^+$···$CuCl_4^{2-}$ contacts as can be seen in the significant reduction of calculated exchange values when the 5-FAP$^+$ cations are introduced into the calculation. Tests done using 1D and 2D alternative magnetic topologies do not satisfactorily reproduce the experimental curve of the magnetic susceptibility and thus demonstrate that the strong correlation to the best-fitting model is fortuitous. First-principles bottom-up calculations indicate the existence of three non-negligible $J(di)$ magnetic pair interactions: -8.21 (-11.8 K), -4.91 (-7.1 K), and -2.44 cm^{-1} (-3.5 K), which agrees well with the crystal packing structure. As a result, the macroscopic experimental antiferromagnetism of $\chi(T)$ is fully reproduced, and the computed spin gap (8.68 K) is also in agreement with the experimental data (11.3 K). Finally, one must emphasize that $(5\text{-FAP})_2CuCl_4$ is an example of a three-dimensional antiferromagnet having a spin gap which prevents spontaneous ordering.

Acknowledgment. We thank Mr. Fan Xiao for assistance in obtaining the magnetic data. We are grateful for grants from the NSF (IMR-0314773) toward the purchase of the MPMS SQUID, from PCISynthesis Inc. toward the purchase of the D8 Powder X-ray Diffractometer, and the Kresge Foundation toward the purchase of both. A portion of this work was performed at the National High Magnetic Field Laboratory, which is supported by NSF Cooperative Agreement No. DMR-0084173, by the State of Florida and by the DOE. The authors also thank the Spanish Science and Education Ministry for support (projects BQU2002-04587-C02-02, CTQ2005-02329, and UNBA05-33-001), the Catalan DURSI (grants 2005SGR-00036 and 2005PEIR-0051/69), and the computer time allocated by CESCA and BSC. M.D. thanks the Spanish Science and Education Ministry for the award of a "Ramón y Cajal" Fellowship. We thank Matthias Troyer (ETH, Zurich) for useful discussions and simulations.

IC701645Y